



Article

Effect of Transition Elements on the Thermal Stability of Glassy Alloys 82Al–16Fe–2TM (TM: Ti, Ni, Cu) Prepared by Mechanical Alloying

Nguyen Thi Hoang Oanh ¹, Do Nam Binh ¹, Dung Dang Duc ², Quyen Hoang Thi Ngoc ¹
and Nguyen Hoang Viet ^{1,*}

- ¹ School of Materials Science and Engineering, Hanoi University of Science and Technology, No 1 Dai Co Viet, Hai Ba Trung, Hanoi 100000, Vietnam; oanh.nguyenthihoang@hust.edu.vn (N.T.H.O.); binhdn@moit.gov.vn (D.N.B.); quyen.hoangthingoc@hust.edu.vn (Q.H.T.N.)
- ² School of Engineering Physics, Hanoi University of Science and Technology, No 1 Dai Co Viet, Hai Ba Trung, Hanoi 100000, Vietnam; dung.dangduc@hust.edu.vn
- * Correspondence: viet.nguyenhoang@hust.edu.vn

Abstract: In the present study, the thermal stability and crystallization behavior of mechanical alloyed metallic glassy Al₈₂Fe₁₆Ti₂, Al₈₂Fe₁₆Ni₂, and Al₈₂Fe₁₆Cu₂ were investigated. The microstructure of the milled powders was characterized by scanning electron microscopy (SEM), X-ray diffraction (XRD), and differential scanning calorimetry (DSC). The results showed remarkable distinction in thermal stability of the alloys by varying only two atomic percentages of transition elements. Among them, Al₈₂Fe₁₆Ti₂ alloy shows the highest thermal stability compared to the others. In the crystallization process, exothermal peaks corresponding to precipitation of fcc-Al and intermetallic phases from amorphous matrix were observed.



Citation: Oanh, N.T.H.; Binh, D.N.; Dang Duc, D.; Hoang Thi Ngoc, Q.; Viet, N.H. Effect of Transition Elements on the Thermal Stability of Glassy Alloys 82Al–16Fe–2TM (TM: Ti, Ni, Cu) Prepared by Mechanical Alloying. *Materials* **2021**, *14*, 3978. <https://doi.org/10.3390/ma14143978>

Academic Editor: Hideki Hosoda

Received: 6 June 2021
Accepted: 12 July 2021
Published: 16 July 2021

Publisher's Note: MDPI stays neutral with regard to jurisdictional claims in published maps and institutional affiliations.



Copyright: © 2021 by the authors. Licensee MDPI, Basel, Switzerland. This article is an open access article distributed under the terms and conditions of the Creative Commons Attribution (CC BY) license (<https://creativecommons.org/licenses/by/4.0/>).

Keywords: Al-based amorphous alloy; thermal stability; mechanical alloying; solid-state transformations

1. Introduction

It is widely known that metallic glasses are novel engineering alloys, which exhibited properties that were different from conventional crystalline materials. The unique properties of metallic glass were originally derived from the random atomic arrangement of metallic glasses [1–4]. Owing to the absence of grain boundaries and crystal defects typically found in crystalline materials, amorphous alloys exhibit excellent mechanical properties. The tensile strength of melt-spun Al–ETM–LTM amorphous ribbons exceeded 1200 MPa [5] (early transition metal (ETM), late transition metal (LTM)), which was approximately three times that of conventional aluminum alloys [2]. The Al-based metallic glasses have a great potential application in the automotive industry, aerospace and military fields, requiring high corrosion resistance, high strength, and a high-specificity elastic modulus [6]. Among the aluminum alloys, iron aluminides containing more than 80% Al are promising candidates for structural applications due to high specific strength and excellent corrosion resistance at elevated temperatures under oxidizing, carburizing, and sulfurizing atmospheres [7]. The addition of Fe in an Al matrix by mechanical alloying technique results in a super-saturated solution formation during the milling process and in amorphous Al–Fe alloys in final production [6]. Normally, metallic glasses are metastable materials at room temperature. Under a suitable heating process, the atoms rearrange to form crystalline or quasicrystalline phases [1,4,8–10]. The crystallization behavior of Al–Ni–La ternary [11] and Al–Fe–Ni–La quaternary [12] systems indicated a three-stage process with primary crystallization of the fcc–Al. It has been noticed that the homogeneous dispersion of nanocrystalline fcc–Al particles in the residual amorphous matrix increase in tensile strength up to 1560 MPa, as reported in [13]. Despite the remarkable

improvement of tensile strength of the amorphous materials, the limited ductility can be incorporated into the amorphous matrix through the dispersion of nanometric phases [4,9,14]. N. Bassim et al. [15] studied the crystallization behavior and microstructure development upon annealing amorphous melt-spun ribbons $\text{Al}_{84}\text{Y}_9\text{Ni}_5\text{Co}_2$. The crystallization onset temperature of this alloy, at a heating rate of 20 K/min, was 292 °C. J. Q. Wang et al. [16] investigated the crystallization behavior of as-quenched $\text{Al}_{88}\text{Ni}_9\text{Ce}_2\text{Fe}_1$ melt-spun ribbons. The first crystallization reaction with precipitation of nanocrystals had an onset temperature of 155.2 °C. Additionally, Viet et al. [17] studied the crystallization kinetics of Al–Fe and Al–Fe–Y amorphous alloys synthesized by mechanical alloying. It was reported that the crystallization onset temperatures can be increased with an increase in the Fe content and substitution of Y for Al. However, only a few works have studied the thermal stability and crystallization behavior of the Al–Fe–TM (transition metal (TM)) alloys prepared by mechanical alloying (MA) to date. Some practical techniques synthesize amorphous alloys with metastable equilibrium microstructures, such as mechanical alloying (MA), melt spinning, gas atomization, and rapid quenching techniques [4,9,18–24]. Among them, MA is a versatile method owing to its simplicity and ease of synthesis. The MA products are produced in powder form, which is very helpful for the sintering process. In addition, MA also extends solid solubility in many binary systems, which are normally immiscible in the solid state or even in the liquid state [9,25–27].

In this work, the thermal stability of metallic glasses alloys with a nominal composition of $\text{Al}_{82}\text{Fe}_{16}\text{Ti}_2$, $\text{Al}_{82}\text{Fe}_{16}\text{Ni}_2$, and $\text{Al}_{82}\text{Fe}_{16}\text{Cu}_2$ prepared by mechanical alloying is investigated. The effect of minor alloying additions (Ti, Ni, Cu) on crystallization and thermal stability of Al–Fe alloys is also examined.

2. Materials and Methods

82Al–16Fe–2TM (TM: Ti, Ni, Cu) amorphous alloy powders were prepared by mechanical alloying from elemental blend powders in a Fritsch Pulverisette-6 (Fritsch, Idar-Oberstein, Germany) planetary ball mill at a rotation rate of 300 rpm, according to our previous work [28]. Hardened steel balls were used at a 20:1 ball to powder weight ratio. Stainless steel vials were used to contain the powder and milling balls, and 50 mL of n-hexane was added as a control agent to prevent sticking phenomena. Before milling, the vials were sealed and evacuated. The milling processes were interrupted every 30 min to prevent excessive heating. In order to investigate the thermal stability, three alloy powders, after milling for 10, 40, 50, and 60 h in amorphous state, corresponding to $\text{Al}_{82}\text{Fe}_{16}\text{Ti}_2$, $\text{Al}_{82}\text{Fe}_{16}\text{Ni}_2$, and $\text{Al}_{82}\text{Fe}_{16}\text{Cu}_2$, respectively, were chosen.

The morphology of milled powders was characterized by field-emission scanning electron microscopy (FE-SEM) using a JEOL JSM-7600F (JEOL Ltd., Tokyo, Japan). Phase analysis was done by X-ray diffraction (XRD) in a SIEMENS D5000 diffractometer (Siemens, Berlin, Germany) using Cu $K\alpha$ radiation ($\lambda = 1.5405 \text{ \AA}$). The XRD parameters were: 2θ range of 20 to 80°; a step size of 0.03°; scanning speed 1° per min. Particle size distribution of amorphous powders was tested by the Laser Scattering Particle Size Distribution Analyzer LA-960 (Horiba Ltd., Kyoto, Japan). The MDI Jade version 6.5 (associated with the ICDD PDF2 database, 2007, Newtown Square, PA, USA) was used for the peaks matching the reference sample. The refined lattice parameters of crystallization phases were evaluated via Profex (version 4.3.2a, released 30 March 2021, Solothurn, Switzerland), a graphical user interface for Rietveld refinement of powder X-ray diffraction data with the program BGMN [29]. The thermal stability of as-milled powders was studied by differential scanning calorimetry (DSC) in a Netzsch STA 449C–QMS 403C Thermal Analyzer System (Netzsch Gerätebau GmbH, Selb, Germany). The non-isothermal DSC studies were carried out at a heating rate of 20 K/min under a continuous flow of purified argon gas flow. Specimens after heating in the calorimeter were investigated by XRD.

3. Results

Figure 1 shows the FE-SEM micrographs of mechanically alloyed powders, $\text{Al}_{82}\text{Fe}_{16}\text{Ti}_2$, $\text{Al}_{82}\text{Fe}_{16}\text{Ni}_2$, and $\text{Al}_{82}\text{Fe}_{16}\text{Cu}_2$, after 40, 50, and 60 h of milling, respectively. In two alloys, $\text{Al}_{82}\text{Fe}_{16}\text{Ti}_2$ and $\text{Al}_{82}\text{Fe}_{16}\text{Ni}_2$, the particle size was about 2 to 3 μm under the SEM observation. Most particles were flattened because of the collision between powders, balls, and jar. The powder particles had a layered structure due to the repeated fracture and welding processes during the milling process. The agglomerate of small powder particles can be seen in Figure 1a,b. In the $\text{Al}_{82}\text{Fe}_{16}\text{Cu}_2$ alloy, the particle size of powder was in the range of 2–10 μm , which implies that the welding process was more dominant. As reported in [28], $\text{Al}_{82}\text{Fe}_{16}\text{Ti}_2$ and $\text{Al}_{82}\text{Fe}_{16}\text{Ni}_2$ alloys are fully amorphous structures after milling for 40 and 50 h, respectively. In $\text{Al}_{82}\text{Fe}_{16}\text{Cu}_2$ powder, only partly amorphous structure was obtained even after milling for a longer time of 60 h. Particle size distribution curves of amorphous alloy samples were measured by means of laser light scattering granulometry, as shown in Figure 2. Two samples exhibited a unimodal distribution and an average particle size, $d_{0.5}$, of 15.9 and 9.4 μm for $\text{Al}_{82}\text{Fe}_{16}\text{Ti}_2$ and $\text{Al}_{82}\text{Fe}_{16}\text{Ni}_2$ powders after 40 and 50 h of milling, respectively. Meanwhile, the $\text{Al}_{82}\text{Fe}_{16}\text{Cu}_2$ alloy sample exhibited a bimodal distribution and an average particle size, $d_{0.5}$, of 14.6 μm . Figure 2d compares the cumulative size distribution curve of three alloy powders. While the particle size distribution of $\text{Al}_{82}\text{Fe}_{16}\text{Ni}_2$ and $\text{Al}_{82}\text{Fe}_{16}\text{Cu}_2$ remained nearly the same in the lower size range, the cumulative size distribution curve of $\text{Al}_{82}\text{Fe}_{16}\text{Ti}_2$ shifted rightwards, indicating that particle size shifted to a larger micron range (<30 μm at 90% volume fraction).

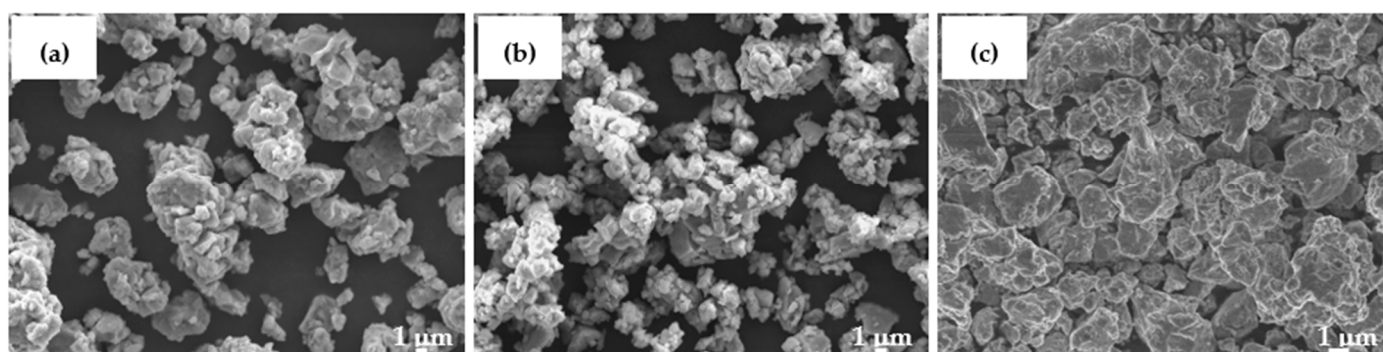


Figure 1. FE-SEM micrographs of (a) $\text{Al}_{82}\text{Fe}_{16}\text{Ti}_2$, (b) $\text{Al}_{82}\text{Fe}_{16}\text{Ni}_2$, and (c) $\text{Al}_{82}\text{Fe}_{16}\text{Cu}_2$ powders after 40, 50, and 60 h of milling, respectively.

Table 1 listed atomic radii mismatch (in %) and enthalpies of mixing (in kJ/mole) for Al, Fe, Ni, Ti, Cu, Y, and La binary systems, according to [30,31]. The three basic empirical rules, for the achievement of high glass-forming ability, are: (1) the alloy must contain at least three components; (2) a significant atomic size difference among the main constituent elements in the alloy should be above 12%; (3) there should be a negative heat of mixing among the major constituent elements in the alloy system [32,33]. The three rules played an important role in the selection of elements for bulk metallic glasses containing rare-earth alloys fabricated by rapid quenching technique. However, there are cases where those rules do not apply, namely for metallic glass alloys containing rare-earth elements and produced by mechanical alloying, such as $\text{Al}_{82}\text{Fe}_{16}\text{Y}_2$ and $\text{Al}_{82}\text{Fe}_4\text{Ni}_4\text{La}_{10}$ systems. Y and La have quite large atomic sizes, and the atomic mismatches of Al–Y and Al–La are about 21.4 and 23.9%, respectively. These alloys achieved a fully amorphous structure for a long time of milling at 100 and 350 h, respectively [12,17]. In contrast, the amorphization of Al–Fe alloys without rare-earth elements, such as $\text{Al}_{82}\text{Fe}_{16}\text{Ti}_2$, $\text{Al}_{82}\text{Fe}_{16}\text{Ni}_2$, and $\text{Al}_{82}\text{Fe}_{16}\text{Cu}_2$, occurs after shorter milling periods [28]. It is evident that the atomic mismatch does not significantly influence the glass-forming ability (GFA) in Al–Fe alloys produced by the mechanical alloying technique because of the nearly similar atomic size of Ti, Ni, and Cu transition elements. However, the amorphization process varied with the mixing enthalpy

values of transition elements. This could be due to the values of the different mixing enthalpy of different alloying elements in ascending orders: Al–Ti < Al–Ni < Al–Cu, as well as Fe–Ti < Fe–Ni < Fe–Cu. There is a tendency for glass formation to increase with decreasing mixing enthalpy. The $\text{Al}_{82}\text{Fe}_{16}\text{Ti}_2$ alloy presented the most negative mixing enthalpy with all binary elements, while Ni has a small negative value of mixing enthalpy with Fe, and Cu showed a positive enthalpy of mixing with Fe. The values of mixing enthalpy may be decisive in the amorphization process.

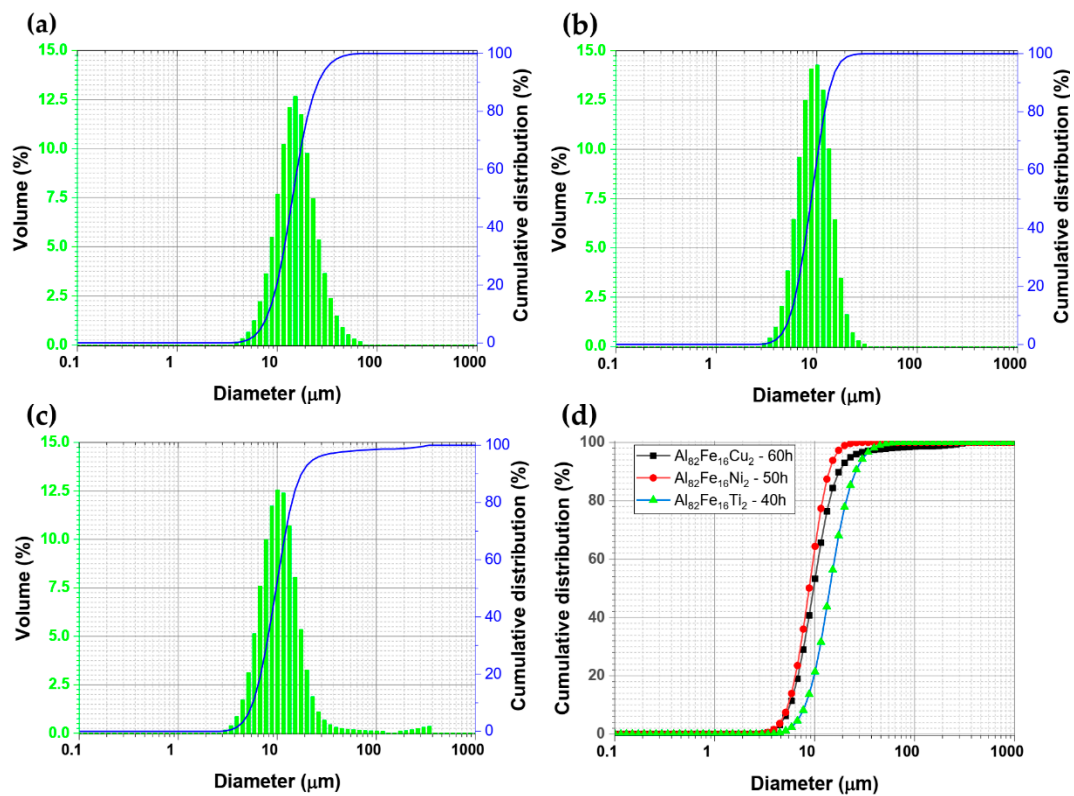


Figure 2. Particle size distribution of (a) $\text{Al}_{82}\text{Fe}_{16}\text{Ti}_2$, (b) $\text{Al}_{82}\text{Fe}_{16}\text{Ni}_2$, and (c) $\text{Al}_{82}\text{Fe}_{16}\text{Cu}_2$ powders after 40, 50, and 60 h of milling, respectively; (d) cumulative distribution of three alloy powders.

Table 1. Atomic radii mismatch (in %) and enthalpies of mixing (in kJ/mole) for Al, Fe, Ni, Ti, Cu, Y, and La binary systems [30].

Element	Al	Fe	Ti	Ni	Cu	Y	La
Al	-	13 (%)	2.7 (%)	12.5 (%)	10 (%)	21.4 (%)	23.9 (%)
Fe	−11 (kJ/mole)	-	15.6 (%)	0.8 (%)	3.1 (%)	31.8 (%)	34 (%)
Ti	−30 (kJ/mole)	−17 (kJ/mole)	-	14.9 (%)	12.9 (%)	19.2 (%)	21.8 (%)
Ni	−22 (kJ/mole)	−2 (kJ/mole)	−35 (kJ/mole)	-	2.3 (%)	31.3 (%)	33 (%)
Cu	−1 (kJ/mole)	+4 (kJ/mole)	−9 (kJ/mole)	+4 (kJ/mole)	-	29.6 (%)	31.9 (%)
Y	−38 (kJ/mole)	−1 (kJ/mole)	+15 (kJ/mole)	−31 (kJ/mole)	−22 (kJ/mole)	-	3 (%)
La	−38 (kJ/mole)	+5 (kJ/mole)	+20 (kJ/mole)	−27 (kJ/mole)	−21 (kJ/mole)	+20 (kJ/mole)	-

In order to investigate the thermal stability of the as-milled powders, a non-isothermal DSC mode was applied. Figure 3a–c presented the DSC curves of milled powders after 10 h and amorphous states of milling, respectively. Characteristic temperatures, T_x and T_p (onset and maximum of the crystallization exothermic peak, respectively), were obtained from DSC scans of powdered samples heated at a constant heating rate of $20 \text{ K}\cdot\text{min}^{-1}$. Most DSC curves of three alloy powders milled at different times exhibited three exothermic peaks, except $\text{Al}_{82}\text{Fe}_{16}\text{Cu}_2$ alloy powders milled for 10 h. The calorimetric curve recorded

for this alloy presented only one peak at a temperature of about 320–420 °C. From the XRD patterns of powders milled for 10 h, there was a small broad diffuse halo of an amorphous phase together with sharpness diffraction peaks corresponding to the existence of minor volume fractions of unprocessed nanoparticles in a scattering range of 2θ between 40–50°, as presented in our previous work [28]. These nanoparticles reacted with each other to produce intermetallic phases, resulting in lower onset crystallization temperatures of three alloys. The onset temperature of amorphous $\text{Al}_{82}\text{Fe}_{16}\text{Ti}_2$, $\text{Al}_{82}\text{Fe}_{16}\text{Ni}_2$, and $\text{Al}_{82}\text{Fe}_{16}\text{Cu}_2$ alloys after milling for 40, 50, and 60 h starts at 398, 365, and 334 °C, respectively. The $\text{Al}_{82}\text{Fe}_{16}\text{Ti}_2$ alloy had the highest onset crystallization temperature, and the $\text{Al}_{82}\text{Fe}_{16}\text{Cu}_2$ alloy had the lowest onset temperature. This DSC profile was similar to the one reported in the literature for $\text{Al}_{82}\text{Fe}_{18}$ and $\text{Al}_{82}\text{Fe}_{16}\text{Y}_2$ alloy [34], where the peaks are related to the exothermic effects connected with fcc-Al and intermetallic phases.

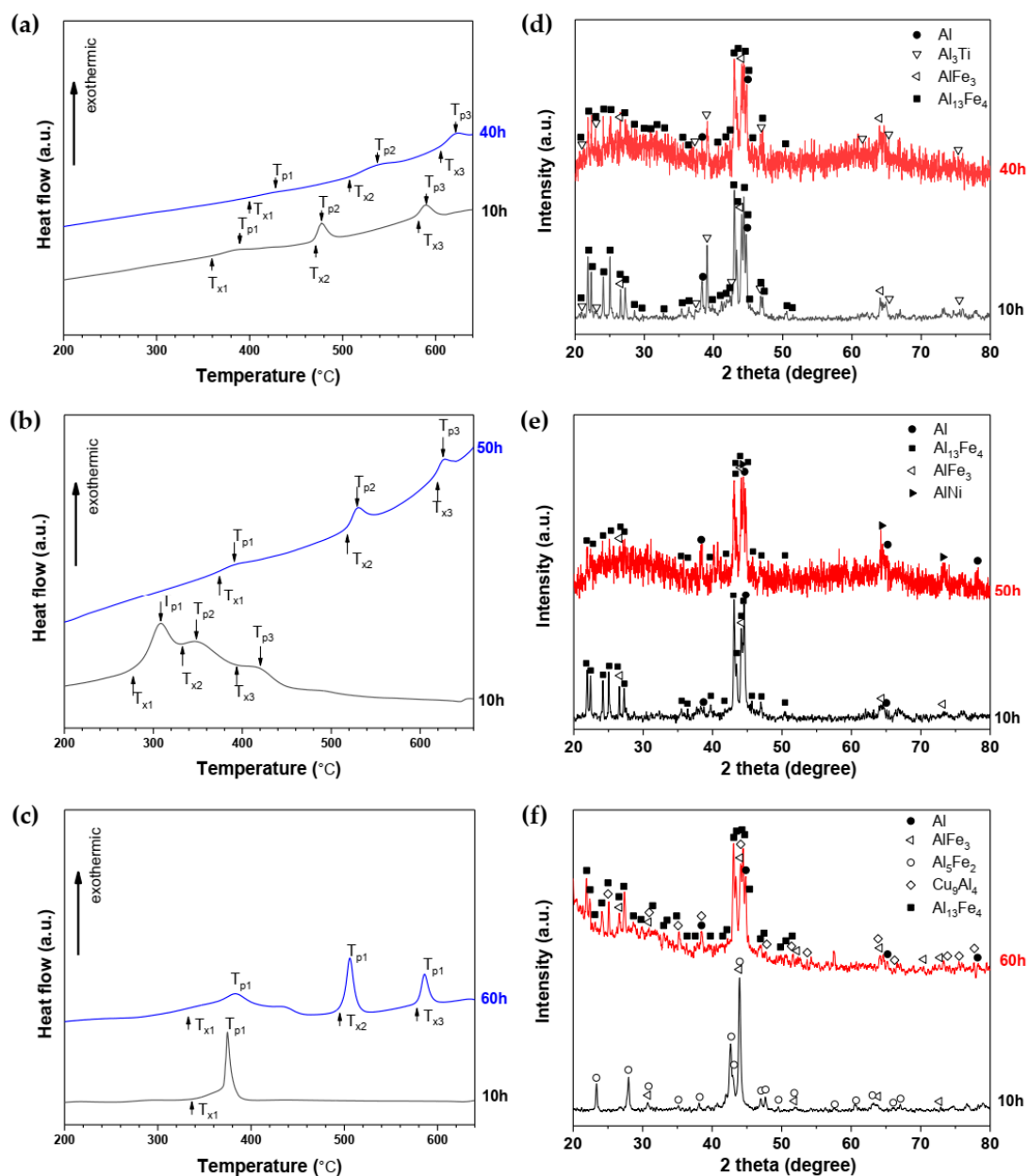


Figure 3. DSC curves of as-milled (a) $\text{Al}_{82}\text{Fe}_{16}\text{Ti}_2$, (b) $\text{Al}_{82}\text{Fe}_{16}\text{Ni}_2$, and (c) $\text{Al}_{82}\text{Fe}_{16}\text{Cu}_2$ alloy powders and their XRD patterns after DSC examination of (d) $\text{Al}_{82}\text{Fe}_{16}\text{Ti}_2$, (e) $\text{Al}_{82}\text{Fe}_{16}\text{Ni}_2$, and (f) $\text{Al}_{82}\text{Fe}_{16}\text{Cu}_2$ alloys.

The thermal stability of three amorphous alloys can be explained by the binary mixing enthalpies of constituent elements listed in Table 1. ΔH_{mix} between Ti, Ni, Cu, and Al (solvent) is -30 , -22 and -1 kJ/mole, respectively. Thus, ΔH_{mix} of Ti–Al was more negative than that of Ni–Al and Cu–Al. The crystallization onset temperature of the $\text{Al}_{82}\text{Fe}_{16}\text{Ti}_2$ amorphous alloy was the highest value among the three alloys. The more negative the enthalpy of mixing, the larger the atomic constraint force, resulting in a higher thermal stability. The thermal stabilities of the three alloys were in the following order: $\text{Al}_{82}\text{Fe}_{16}\text{Ti}_2$ – $\text{Al}_{82}\text{Fe}_{16}\text{Ni}_2$ – $\text{Al}_{82}\text{Fe}_{16}\text{Cu}_2$. Looking into details of the other alloys in Table 2, we can see that amorphous $\text{Al}_{84}\text{Fe}_{16}$ composition starts crystallization at 353 °C. The substitution of Fe for Al (2 at.%) in $\text{Al}_{84}\text{Fe}_{16}$, the alloy system became $\text{Al}_{82}\text{Fe}_{18}$ and the number of Al–Fe pairs increased from 16 to 18. The crystallization temperature of $\text{Al}_{82}\text{Fe}_{18}$ was raised to 375 °C. As the number of Al–Fe pairs increased, the thermal stability of $\text{Al}_{82}\text{Fe}_{18}$ alloy also increased. Similar to the above case, the substitution of Ti for Al (2 at.%) results in the crystallization onset temperature of the $\text{Al}_{82}\text{Fe}_{16}\text{Ti}_2$ alloy, increasing to 398 °C. ΔH_{mix} of Ti–Fe (-17 kJ/mole) was more negative than that of Al–Fe (-1 kJ/mole), which means that the GFA of the $\text{Al}_{82}\text{Fe}_{16}\text{Ti}_2$ alloy can be improved more compared to that of the $\text{Al}_{84}\text{Fe}_{16}$ alloy. However, in the $\text{Al}_{82}\text{Fe}_{16}\text{Ni}_2$ alloy, the crystallization temperature was higher than $\text{Al}_{84}\text{Fe}_{16}$ and lower than $\text{Al}_{82}\text{Fe}_{18}$ and $\text{Al}_{82}\text{Fe}_{16}\text{Ti}_2$ alloys. ΔH_{mix} of Ni–Fe is (-2 kJ/mole) was lower than Al–Fe (-11 kJ/mole) and Ti–Fe (-17 kJ/mole), which results in the lower crystallization temperature of the $\text{Al}_{82}\text{Fe}_{16}\text{Ni}_2$ alloy, compared to $\text{Al}_{84}\text{Fe}_{16}$, $\text{Al}_{82}\text{Fe}_{18}$, and $\text{Al}_{82}\text{Fe}_{16}\text{Ti}_2$ alloys. DSC curves of the $\text{Al}_{82}\text{Fe}_{16}\text{Cu}_2$ alloy showed very broad peaks between 120 and 700 °C, similar to the $\text{Al}_{75}\text{Fe}_{25}$ alloy, as reported in [33]. The $\text{Al}_{82}\text{Fe}_{16}\text{Cu}_2$ alloy had the lowest crystallization temperature due to its partial amorphous structure. It was found that the GFA reduced with the addition of Cu in $\text{Al}_{84}\text{Fe}_{16}$ due to the positive mixing enthalpies of Fe–Cu ($+13$ kJ/mole). The more negative the mixing enthalpy in the alloy, the more thermally stable an amorphous phase against solid solution and intermediate phase is [35]. Z. Zhang et al. investigated Al–Ni–RE (RE–La, Ce) alloys produced by arc melting, which exhibited a strong dependence on the size of the RE atom and negative mixing enthalpy between the constituent elements with the glass formation [36]. However, Al–Fe–2TM prepared by MA showed that the most important factor, decided by the GFA of the alloys, was a larger negative mixing enthalpy between the constituent elements.

Table 2. Crystallization temperatures and phase compositions of Al–Fe alloys produced by a planetary ball mill.

Alloys	Phase after MA	Crystallization Temperatures, (°C)							Crystallization Phases	Ref
		T _{x1}	T _{p1}	T _{x2}	T _{p2}	T _{x3}	T _{p3}	T _{x4}		
$\text{Al}_{84}\text{Fe}_{16}$	amorphous	353	-	450	-	511	-	590	Al, $\text{Al}_{13}\text{Fe}_4$, Al_6Fe	[34]
$\text{Al}_{82}\text{Fe}_{18}$	amorphous	380	-	491	-	579	-	-	Al, $\text{Al}_{13}\text{Fe}_4$	[34]
$\text{Al}_{82}\text{Fe}_{16}\text{Y}_2$	amorphous	382	-	486	-	584	-	-	Al, Al_6Fe , Fe_4Y , $\text{Al}_{13}\text{Fe}_4$	[34]
$\text{Al}_{82}\text{Fe}_{16}\text{Ti}_2$	amorphous	398	424	507	535	605	623	-	Al, Al_3Ti , AlFe_3 , $\text{Al}_{13}\text{Fe}_4$	This work
$\text{Al}_{82}\text{Fe}_{16}\text{Ni}_2$	amorphous	365	393	516	530	617	627	-	Al, $\text{Al}_{13}\text{Fe}_4$, AlFe_3 , AlNi	This work
$\text{Al}_{82}\text{Fe}_{16}\text{Cu}_2$	Partly amorphous	334	382	495	506	576	586	-	Al, $\text{Al}_{13}\text{Fe}_4$, AlFe_3 , Al_5Fe_2 , Cu_9Al_4	This work

The phase transformation of amorphous alloy powders after DSC heating was performed by using the XRD technique. The X-ray diffraction patterns of the DSC-quenched samples for as-milled $\text{Al}_{82}\text{Fe}_{16}\text{Ti}_2$, $\text{Al}_{82}\text{Fe}_{16}\text{Ni}_2$, and $\text{Al}_{82}\text{Fe}_{16}\text{Cu}_2$ alloy powders are shown in Figure 3d–f. Similar phase formations were seen in $\text{Al}_{82}\text{Fe}_{16}\text{Ti}_2$ and $\text{Al}_{82}\text{Fe}_{16}\text{Ni}_2$ alloys

after being milled for 10, 40, and 50 h. However, for $\text{Al}_{82}\text{Fe}_{16}\text{Cu}_2$ alloy powder milled for 10 h, only Al_5Fe_2 and AlFe_3 were detected from XRD patterns, while higher precipitation phases of fcc-Al, Cu_9Al_4 , and $\text{Al}_{13}\text{Fe}_4$ could be only obtained from $\text{Al}_{82}\text{Fe}_{16}\text{Cu}_2$ alloy powder milled for 60 h.

Via the thermal effect, the glassy phase was transformed into fcc-Al and intermetallic phases. The first exothermic peak around 360–390 °C represents the precipitation of crystalline α -Al on the Al matrix, which could improve the strength of the alloy and increase material performance [24]. The next two exothermal peaks mark the appearance of intermetallic phases, such as $\text{Al}_{13}\text{Fe}_4$, AlFe_3 , and Al_3Ti for the $\text{Al}_{82}\text{Fe}_{16}\text{Ti}_2$ alloy; AlNi , AlFe_3 , and $\text{Al}_{13}\text{Fe}_4$ for $\text{Al}_{82}\text{Fe}_{16}\text{Ni}_2$ alloy; and Cu_9Al_4 , Al_5Fe_2 , AlFe_3 , and $\text{Al}_{13}\text{Fe}_4$ for the $\text{Al}_{82}\text{Fe}_{16}\text{Cu}_2$ alloy. These intermetallic phases have negative formation enthalpy as the Miedema calculation [37]. The formation enthalpies of $\text{Al}_{13}\text{Fe}_4$, AlFe_3 , Al_3Ti , Al_5Fe_2 , AlNi , and Cu_9Al_4 are -18.052 , -22.078 , -39.02 , -21.855 , -48.424 , and -13.104 kJ/mole, respectively. A mixture of $\text{Al}_{13}\text{Fe}_4$, Al_6Fe , Fe_4Y , and Al phases was reported as a crystallization product after heating the amorphous $\text{Al}_{82}\text{Fe}_{16}\text{Y}_2$ alloy to 700 °C in the same calorimeter used in previous our work [34]. It can be realized that, for amorphous alloys with a small amount of the different transition elements or rare-earth elements obtained in the same mills, dissimilar phases crystallized during analogous heat treatment. Thus, the crystallization process of amorphous alloys with the same milling parameters can be influenced by composition. This indicates that these Al-based amorphous alloys (produced in the same mills) actually differ. The refined lattice parameters of the DSC-quenched samples were calculated using Profex software packages. It is very interesting that two $\text{Al}_{13}\text{Fe}_4$ and AlFe_3 intermetallic phases were precipitated from the amorphous phase of all three alloys. Considering this, milling of these alloys resulted in the formation of solid solutions of α -Al(Fe) and α -Fe(Al), then transformed to the AlFe_3 intermetallic phase. Additionally, in the opposite process, the crystallization of the amorphous phase, the AlFe_3 intermetallic phase was also produced. It is noticeable that the AlFe_3 phase had high negative formation enthalpy of -22.078 kJ/mole, so it was easy to form during crystallization. A slight difference in lattice parameters for $\text{Al}_{13}\text{Fe}_4$ and AlFe_3 intermetallic phases can be seen in Table 3. A lattice expansion is observed as a result of disordering of the lattice when the iron diffusion into the aluminum lattice formed intermetallic phases during crystallization. The lattice constant of fcc-Al as a sample after DSC was similar to that in #PDF 04-0787.

Table 3. Refined lattice parameters of crystallization phases formed from DSC-quenched $\text{Al}_{82}\text{Fe}_{16}\text{Ti}_2$, $\text{Al}_{82}\text{Fe}_{16}\text{Ni}_2$, and $\text{Al}_{82}\text{Fe}_{16}\text{Cu}_2$ alloy powders.

Sample	Phase	ICDD/JCPDS ID *	Lattice Parameters (nm)	CIF ID **	Refined Lattice Parameters (nm)		Formation Enthalpy, kJ/mol
$\text{Al}_{82}\text{Fe}_{16}\text{Ti}_2$ Cubic, <i>Fm</i> -3 <i>m</i> (225)	Al	04-0787	$a = 0.40494$		MA 10 h	MA 40 h	
			$a = 1.5489$		$a = 0.40584$	$a = 0.4049$	
Monoclinic <i>C2/m</i> (12)	$\text{Al}_{13}\text{Fe}_4$	29-0042	$b = 0.8083$	ICSD_151129	$a = 1.5498$	$a = 1.5511$	-18.052
			$c = 1.2476$		$b = 0.8089$	$b = 0.8092$	
			$\beta = 107.7$		$c = 1.2501$	$c = 1.2527$	
Cubic <i>Fm</i> -3 <i>m</i> (225)	AlFe_3	45-1203	$a = 0.57934$	mp-2018	$\beta = 107.93$	$\beta = 108.15$	-22.078
			$a = 0.5765$		$a = 0.5803$		
Tetragonal <i>I4/mmm</i> (139)	Al_3Ti	37-1449	$a = 0.38537$	mp-542915	$a = 0.3851$	$a = 0.3852$	-39.020
			$c = 0.85839$		$c = 0.8602$	$c = 0.8609$	

Table 3. Cont.

Sample	Phase	ICDD/JCPDS ID *	Lattice Parameters (nm)	CIF ID **	Refined Lattice Parameters (nm)		Formation Enthalpy, kJ/mol	
$\text{Al}_{82}\text{Fe}_{16}\text{Ni}_2$ Cubic <i>Fm-3m</i> (225)	Al	-	$a = 0.40494$	-	MA 10 h	MA 50 h	-	
			$a = 1.5489$		$a = 0.4053$	$a = 0.4049$	-	
	Monoclinic <i>C2/m</i> (12)	$\text{Al}_{13}\text{Fe}_4$	29-0042	$b = 0.8083$ $c = 1.2476$ $\beta = 107.7$	ICSD_151129	$a = 1.5462$ $b = 0.8118$ $c = 1.2489$ $\beta = 107.81$	$a = 1.5495$ $b = 0.8084$ $c = 1.2491$ $\beta = 107.89$	-
Cubic <i>Fm-3m</i> (225)	AlFe_3	50-0955	$a = 0.58152$	mp-2018	$a = 0.5747$	$a = 0.5803$	-	
$\text{Al}_{82}\text{Fe}_{16}\text{Cu}_2$ Cubic <i>Fm-3m</i> (225)	Al	-	$a = 0.40494$	-	MA 10 h	MA 60 h	-	
			$a = 1.5489$		-	$a = 0.4050$	-	
	Monoclinic <i>C2/m</i> (12)	$\text{Al}_{13}\text{Fe}_4$	29-0042	$b = 0.8083$ $c = 1.2476$ $\beta = 107.7$	ICSD_151129	-	$a = 1.5515$ $b = 0.8094$ $c = 1.2521$ $\beta = 107.86$	-
	Cubic <i>Fm-3m</i> (225)	AlFe_3	50-0955	$a = 0.58152$	mp-2018	$a = 0.5803$	$a = 0.5771$	-
	Orthorhombic <i>Cmcm</i> (63)	Al_5Fe_2	47-1435	$a = 0.76486$ $b = 0.64131$ $c = 0.42165$	COD_2101159	$a = 0.7620$ $b = 0.6424$ $c = 0.4204$	-	-21.855
Cubic <i>P-43m</i> (215)	Cu_9Al_4	24-0003	$a = 0.87027$	mp-593	-	$a = 0.8789$	-13.104	

* id of materials taken from ICDD/JCPDS were indexed in MDI Jade 6.5. ** id of materials were taken from materialsproject.org, www.crystallography.net (accessed on 7 August 2020), and icsd.products.fiz-karlsruhe.de, which were then converted to structure files used in Profex software.

4. Conclusions

In the present study, the thermal stability of mechanically alloying powders increased in the order of $\text{Al}_{82}\text{Fe}_{16}\text{Cu}_2$, $\text{Al}_{82}\text{Fe}_{16}\text{Ni}_2$, and $\text{Al}_{82}\text{Fe}_{16}\text{Ti}_2$ alloys. The crystallization in $\text{Al}_{82}\text{Fe}_{16}\text{Ti}_2$, $\text{Al}_{82}\text{Fe}_{16}\text{Ni}_2$, and $\text{Al}_{82}\text{Fe}_{16}\text{Cu}_2$ started at: 398, 365, and 334 °C, respectively. For ternary Al–Fe–TM (TM: Ti, Ni, Cu) alloys, ΔH_{mix} was the main factor deciding the amorphization process. The larger the negative mixing enthalpy between binary elements in the alloys, the faster the amorphization process was. $\text{Al}_{82}\text{Fe}_{16}\text{Ti}_2$ amorphous alloy had the highest glass-forming ability and thermal stability among the three alloys. A considerably lower thermal stability of $\text{Al}_{82}\text{Fe}_{16}\text{Cu}_2$ than the other alloys may arise from a system with a positive heat of mixing. A larger negative mixing enthalpy between the constituent elements was the key factor, which decided the GFA of amorphous alloys. The crystallization of these alloys occurred during the DSC process, with the transformation of the amorphous phase into fcc-Al and intermetallic phases. The diffusion of Fe in Al lattice to produce intermetallic phase $\text{Al}_{13}\text{Fe}_4$ and AlFe_3 resulted in the slightly different lattice parameters compared to standard phases. The GFA and crystallization in Al–Fe–2TM metallic glasses were much more sensitive to minor alloying elements.

Author Contributions: Conceptualization, N.H.V., N.T.H.O., and D.N.B.; methodology, investigation, and validation, D.N.B. and Q.H.T.N.; software, visualization, and validation, D.D.D., Q.H.T.N. and N.H.V.; writing—original draft preparation, review, and editing, N.T.H.O., D.D.D. and N.H.V. All authors have read and agreed to the published version of the manuscript.

Funding: This research is funded by the Hanoi University of Science and Technology (HUST) under project number T2020-TĐ-007.

Institutional Review Board Statement: Not applicable.

Informed Consent Statement: Not applicable.

Data Availability Statement: Data is contained within the article.

Conflicts of Interest: The authors declare no conflict of interest.

References

1. He, Y.; Poon, S.J.; Shiflet, G.J. Synthesis and Properties of Metallic Glasses That Contain Aluminum. *Science* **1988**, *241*, 1640. [[CrossRef](#)]
2. He, Y.; Shiflet, G.J.; Poon, S.J. Synthesis and properties of aluminum-based metallic glasses containing rare earths. *J. Alloys Compd.* **1994**, *207–208*, 349–354. [[CrossRef](#)]
3. Miller, M.K.; Liaw, P. *Bulk Metallic Glasses*; Springer: New York, NY, USA, 2008; p. 256.
4. Suryanarayana, C.; Inoue, A. Metallic Glasses. In *Ullmann's Encyclopedia of Industrial Chemistry*; Wiley-VCH Verlag GmbH: Weinheim, Germany, 2012. [[CrossRef](#)]
5. Eckert, J.; Calin, M.; Yu, P.; Zhang, L.C.; Scudino, S.; Duhamel, C. Al-based alloys containing amorphous and nanostructured phases. *Rev. Adv. Mater. Sci.* **2008**, *18*, 169–172.
6. Seikh, A.H.; Baig, M.; Singh, J.K.; Mohammed, J.A.; Luqman, M.; Abdo, H.S.; Khan, A.R.; Alharthi, N.H. Microstructural and Corrosion Characteristics of Al-Fe Alloys Produced by High-Frequency Induction-Sintering Process. *Coatings* **2019**, *9*, 686. [[CrossRef](#)]
7. Krasnowski, M.; Kulik, T. Nanocrystalline and amorphous Al-Fe alloys containing 60–85% of Al synthesised by mechanical alloying and phase transformations induced by heating of milling products. *Mater. Chem. Phys.* **2009**, *116*, 631–637. [[CrossRef](#)]
8. Inoue, A.; Kimura, H. Fabrications and mechanical properties of bulk amorphous, nanocrystalline, nanoquasicrystalline alloys in aluminum-based system. *J. Light Met.* **2001**, *1*, 31–41. [[CrossRef](#)]
9. Suryanarayana, C. Mechanical Alloying: A Novel Technique to Synthesize Advanced Materials. *Research* **2019**, *2019*, 4219812. [[CrossRef](#)]
10. Inoue, A.; Kong, F.; Zhu, S.; Liu, C.; Al-Marzouki, F. Development and Applications of Highly Functional Al-based Materials by Use of Metastable Phases. *Mater. Res.* **2015**, *18*. [[CrossRef](#)]
11. Zhang, Z.; Witkin, D.; Lavernia, E.J. Crystallization behavior of a gas atomized Al₈₅Ni₁₀La₅ amorphous alloy. *J. Non-Cryst. Solids* **2005**, *351*, 1646–1652. [[CrossRef](#)]
12. Viet, N.H.; Oanh, N.T.; Kim, J.-S.; Jorge, A.M. Crystallization Kinetics and Consolidation of Al₈₂La₁₀Fe₄Ni₄ Glassy Alloy Powder by Spark Plasma Sintering. *Metals* **2018**, *8*, 812. [[CrossRef](#)]
13. Kim, H.S.; Hong, S.I.; Kato, H.; Inoue, A. Strengthening Mechanisms in Al-Based and Zr-Based Amorphous Nanocomposites. *Mater. Trans.* **2002**, *43*, 2026–2030. [[CrossRef](#)]
14. Roy, D.; Chakravarty, D.; Mitra, R.; Manna, I. Effect of sintering on microstructure and mechanical properties of nano-TiO₂ dispersed Al₆₅Cu₂₀Ti₁₅ amorphous/nanocrystalline matrix composite. *J. Alloys Compd.* **2008**, *460*, 320–325. [[CrossRef](#)]
15. Bassim, N.; Kiminami, C.S.; Kaufman, M.J.; Oliveira, M.F.; Perdigo, M.N.R.V.; Botta Filho, W.J. Crystallization behavior of amorphous Al₈₄Y₉Ni₅CO₂ alloy. *Mater. Sci. Eng. A* **2001**, *304–306*, 332–337. [[CrossRef](#)]
16. Wang, J.Q.; Chang, X.C.; Hou, W.L.; Hu, Z.Q. Crystallization behaviour of Al-based amorphous alloy and nanocomposites by rapid quenching. *Philos. Mag. Lett.* **2000**, *80*, 349–357. [[CrossRef](#)]
17. Nguyen, V.H.; Nguyen, O.T.H.; Dudina, D.V.; Le, V.V.; Kim, J.-S. Crystallization Kinetics of Al-Fe and Al-Fe-Y Amorphous Alloys Produced by Mechanical Milling. *J. Nanomater.* **2016**, *2016*, 1909108. [[CrossRef](#)]
18. Weeber, A.W.; Bakker, H. Amorphization by ball milling. A review. *Phys. B Condens. Matter* **1988**, *153*, 93–135. [[CrossRef](#)]
19. Lü, L.; Lai, M.O. *Mechanical Alloying*, 1st ed.; Springer: Boston, MA, USA, 1998; p. 276. [[CrossRef](#)]
20. Suryanarayana, C. *Mechanical Alloying and Milling*, 1st ed.; CRC Press: Boca Raton, FL, USA, 2004; p. 488. [[CrossRef](#)]
21. Surreddi, K.B.; Scudino, S.; Nguyen, H.V.; Nikolowski, K.; Stoica, M.; Sakaliyska, M.; Kim, J.S.; Gemming, T.; Vierke, J.; Wollgarten, M.; et al. Spark plasma sintering of gas atomized Al₈₇Ni₈La₅ amorphous powder. *J. Phys. Conf. Ser.* **2009**, *144*, 012079. [[CrossRef](#)]
22. Nguyen, H.-V.; Kim, J.-S.; Kwon, Y.-S.; Kim, J.-C. Amorphous Ti-Cu-Ni-Al alloys prepared by mechanical alloying. *J. Mater. Sci.* **2009**, *44*, 2700–2704. [[CrossRef](#)]
23. Liu, X.; Wang, X.; Si, Y.; Han, F. Glass-Forming Ability and Thermal Properties of Al₇₀Fe_{12.5}V_{12.5}X₅ (X = Zr, Nb, Ni) Amorphous Alloys via Minor Alloying Additions. *Nanomaterials* **2021**, *11*, 488. [[CrossRef](#)] [[PubMed](#)]
24. Babilas, R.; Spilka, M.; Młynarek, K.; Łoński, W.; Łukowiec, D.; Radoń, A.; Kądziołka-Gaweł, M.; Gebara, P. Glass-Forming Ability and Corrosion Resistance of Al₈₈Y_{8-x}Fe_{4+x} (x = 0, 1, 2 at.%) Alloys. *Materials* **2021**, *14*, 1581. [[CrossRef](#)]
25. Oleszak, D. Mechanical alloying—A novel method for synthesis and processing of materials. *Acta Phys. Pol. A* **1999**, *96*, 101–112. [[CrossRef](#)]
26. Shan, L.; Wang, X.; Wang, Y. Extension of Solid Solubility and Structural Evolution in Nano-Structured Cu-Cr Solid Solution Induced by High-Energy Milling. *Materials* **2020**, *13*, 5532. [[CrossRef](#)] [[PubMed](#)]
27. Suñol, J.-J. Mechanical Alloying: Processing and Materials. *Metals* **2021**, *11*, 798. [[CrossRef](#)]
28. Oanh, N.T.H.; Viet, N.H.; Dudina, D.V.; Jorge, A.M.; Kim, J.-S. Structural characterization and magnetic properties of Al₈₂Fe₁₆TM₂ (TM: Ti, Ni, Cu) alloys prepared by mechanical alloying. *J. Non-Cryst. Solids* **2017**, *468*, 67–73. [[CrossRef](#)]
29. Doebelin, N.; Kleeberg, R. Profex: A graphical user interface for the Rietveld refinement program BGMN. *J. Appl. Cryst.* **2015**, *48*, 1573–1580. [[CrossRef](#)]

30. Takeuchi, A.; Inoue, A. Classification of Bulk Metallic Glasses by Atomic Size Difference, Heat of Mixing and Period of Constituent Elements and Its Application to Characterization of the Main Alloying Element. *Mater. Trans.* **2005**, *46*, 2817–2829. [[CrossRef](#)]
31. Takeuchi, A.; Inoue, A. Analyses of characteristics of atomic pairs in ferrous bulk metallic glasses using classification of bulk metallic glasses and pettifor map. *J. Optoelectron. Adv. Mater.* **2006**, *8*, 1679–1684.
32. Suryanarayana, C.; Inoue, A. Iron-based bulk metallic glasses. *Int. Mater. Rev.* **2013**, *58*, 131–166. [[CrossRef](#)]
33. Urban, P.; Cuevas, F.G.; Montes, J.M.; Cintas, J. Solid state amorphization in the Al-Fe binary system during high energy milling. *AIP Conf. Proc.* **2013**, *1569*, 476–479. [[CrossRef](#)]
34. Nguyen, H.V.; Oanh, N.T.H.; Quynh, P.N.D.; Lap, T.Q.; Kim, J.S. Thermal Stability of Amorphous Al-Fe-Y Prepared by Mechanical Alloying. *Mater. Sci. Forum* **2015**, *804*, 271–274. [[CrossRef](#)]
35. Takeuchi, A.; Inoue, A. Calculations of Mixing Enthalpy and Mismatch Entropy for Ternary Amorphous Alloys. *Mater. Trans. JIM* **2000**, *41*, 1372–1378. [[CrossRef](#)]
36. Zhang, Z.; Xiong, X.Z.; Zhou, W.; Li, J.F. Influence of substitution of La by Ce on the glass forming ability and crystallization behavior of Al–Ni–La alloys. *J. Alloys Compd.* **2013**, *576*, 181–186. [[CrossRef](#)]
37. Zhang, R.F.; Zhang, S.H.; He, Z.J.; Jing, J.; Sheng, S.H. Miedema Calculator: A thermodynamic platform for predicting formation enthalpies of alloys within framework of Miedema's Theory. *Comput. Phys. Commun.* **2016**, *209*, 58–69. [[CrossRef](#)]